Journal of the Serbian Society for Computational Mechanics / Vol. 16 / No. 1, 2022 / pp 125-137
(10.24874/jsscm.2022.16.01.09)

THERMAL ANALYSIS OF LAMINAR WATER FLOW OVER A BACKWARD FACING CHANNEL WITH CARBON NANOPARTICLES

Sandip Saha[1], Vallampati Ramachandra Prasad[2*], Osman Anwar Bég[3]

[1] School of Advanced Sciences, Vellore Institute of Technology Chennai, Chennai, Tamil Nadu, India
e-mail: sandip.saha@vit.ac.in
[2] School of Advanced Sciences, Vellore Institute of Technology Vellore, Vellore, Tamil Nadu, India
e-mail: v.ramachandraprasad@vit.ac.in
[3] Department of Aeronautical/Mechanical Engineering, School of Science, Engineering and Environment (SEE), University of Salford, Newton Building, Manchester, M5 4WT, UK
e-mail: o.a.beg@salford.ac.uk
**corresponding author*

Abstract

In the last few years, the thermo-hydraulic simulation of nanofluid flow bifurcation phenomena has become of great interest to researchers and a useful tool in many engineering applications. FVM has been employed in this article to numerically explore the laminar water flow over a backward facing channel with or without carbon nanoparticles (CN). The problem formulated in this paper has been solved by considering the effects of nanoparticle weight percentages ($w\%$), such as 0.00, 0.12, and 0.25 for different Reynolds number (Re). Nusselt number distribution ($Nu(x)$), coefficient of skin friction (C_f), characteristics of pressure drop (Δp), velocity contours, static temperature, pumping power (P_p) and thermal resistance factor (R) have been investigated to know the behavior of thermo-hydraulic flow bifurcation phenomena. The present study shows that the surface temperature and coefficient of heat transfer can be reduced due to the effect of Re or w%. For different w%, it has been found that in the rise in the values of Re causes the increase of vortex length and as a result velocity gradient and Δp arises. Furthermore, it has also been studied that the enhancement of Re causes the increaseof P_p and Δp.

Keywords: Sudden expansion channel, laminar flow, heat transfer, pumping power, thermal enhancement factor.

1. Introduction

Today, researchers around the world are making considerable efforts to provide more effective heat transfer (HT) equipment in many industrial applications such as space and energy technology, electronic, aviation, medical applications. One of the active fields of research is to develop new methods and correct existing ones in order to improve the HT rate in tools and industrial technology. Due to less HT efficiency, the earlier HT applications are no longer active at present. To improve the cooling fluid thermal conductivity, many researchers (Bardenhagen et

al. 2014, Karimipour et al. 2013, Moshizi et al. 2014) have performed research on different types of channels with the use of nanoparticles (Afrouzi et al. 2013, Karimipour et al. 2015, Saha et al. 2021). Moreover, to study the enhancement of HT capacity in cooling system, many researchers (Afrouzi et al. 2013, Sheikholeslami et al. 2016) have investigated the usefulness of nanofluid instead of water. Furthermore, to increase the power generation in power plants, a large number of authors presented that nanofluid is more useful rather than water (Ram Reddy et al. 2013, Akbari et al. 2016). Significant increase of convective HT coefficient without substantial loss of pressure becomes one of the considerable advantage causes for using nanoparticles. To reveal the thermos-physical characteristics of nanofluids, many authors have considered different channel geometries such as backward and forward-facing contracting channels (Alavi et al. 2015), rectangular channel in presence of ribs 8 (Sarlak et al. 2017, Toghraie et al. 2019).

In a micro-channel heat chamber, Peyghambarzadeh et al. (2014) experimentally studied the laminar flow of water nanofluid/co_2 and H_2O-Al_2O_3. They showed that in case of pressure profile, nanofluid becomes more pronounced than pure water. For the boundary conditions of slip and no-slip, Raisi et al. (2011) numerically investigated the characteristics of thermal-phenomena of water nanofluid-copper oxide in a microchannel heat chamber. It was shown in their work that the HT enhances with the increase of Re. In a micro-channel along with wavy walls, Heidary et al. (2010) noted that the rate of HT is increased 50% in use of nanofluids as compared to water. In a rectangular geometry, Jung et al. (2009) also studied the different characteristics of HT of H_2O-Al_2O_3 nanofluid. They revealed that the HT rate would increase by about 32% for 1.8% volume fraction. Numerically, Behnampour et al. (2017) investigated the HT properties of laminar water/AgO nanofluids through a rectangular micro-channel with different types of baffles. For $[0 - 4]$% volume fractions, they concluded that the velocity profile became more prominent with rectangular baffles than other baffles, but the triangular baffles played a major role in thermal augmentation. In a two-dimensional and three-dimensional micro-channel, Akbari (a, b) et al. (2016) numerically solved the HT phenomena of H_2O-Al_2O_3 nanofluid at different baffle heights. They concluded that the increase in thermal conductivity is due to the increase of baffle height and w%.

Using constant thermal boundary condition, Karimipour et al. (2015) investigated the forced HT coefficient of H_2O/Ag nanofluid over a rectangular micro-channel with rectangular baffle. They have shown that increase in the value of Nu_{avg} causes the increase of Re and volume fraction. In presence of different pitches, Gravndyan et al. (2017) numerically studied the thermo-hydraulic phenomena of Water/TiO_2 in a two-dimensional rectangular micro-channel geometry. In their work, it is observed that the increase of Re flow velocity profile becomes more pronounced and complicated. Moreover, Abu (2008) numerically investigated the laminar nanofluids flow through a backward facing channel for volume fraction $[0.05 - 0.2]$%. Furthermore, using nanofluid, various numerical and experimental studies on HT through different types of geometries have been considered by many authors (Parsaiemehr et al. 2018, Li et al. 2016, Andreozzi et al. 2016).

The literature review shows that nanofluid plays a crucial role in the cooling industry for studying different flow characteristics and HT phenomena. It has become more interesting to study the different HT characteristics and pumping power (P_p), when the nanofluid flows through micro-channel geometry. Moreover, researchers are interested in studying the pressure drop and velocity profile with the variation of w, which can be very helpful in various industrial applications. The present study analyzes different characteristics of nanofluid flow phenomena (velocity profile, pressure profile, and pressure drop (Δp)) and thermal behavior of water flow in presence or absence of carbon nanoparticles through a suddenly expanded channel for expansion ratio 3. In this study, different HT characteristics (static temperature profile, skin friction coefficient (C_f), friction factor (f), local Nusselt number (Nu), average Nusselt number (Nu_{avg}), and pumping

power) have been studied with respect to the variation of $w\%$, Reynolds number (Re), and Nusselt number (Nu).

2. Geometry configuration and dimensions

FLUENT computational fluid dynamics (CFD) software has been utilized to configure the geometry [Fig. 1(a, b)] and simulation purpose. Flow is assumed to be viscous, two-dimensional, laminar, nanofluid, steady, Newtonian and incompressible. Inflow velocity (u_{in}), pressure outlet, no-slip and no-penetrationboundary conditions have been imposed on the inlet, outlet, and wall sections. The effects of radiation are negligible. Table 1 describes the properties of nanofluid in accordance with Nikkhah et al. (2015).

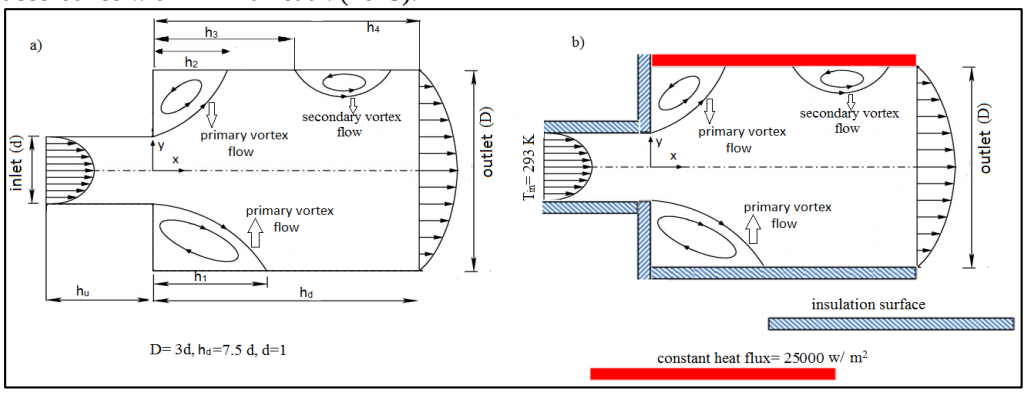

Fig. 1. (a, b) Schematic diagram of a channel with sudden expansion.

3. Mathematical formulations

Newtonian nanofluid flow through a backward-facing channel is governed by the following equation (1) (continuity), equations (2), (3) (momentum), and equation (4) (energy) (Raisi et al. 2014, Mahmoudi et al. 2012, Gholami et al. 2018).

$$\nabla . S = 0 \tag{1}$$

$$S.\nabla u = -\frac{1}{\rho_{nf}}\frac{\partial p}{\partial x} + \frac{\mu_{nf}}{\rho_{nf}}\nabla^2 u \tag{2}$$

$$S.\nabla v = -\frac{1}{\rho_{nf}}\frac{\partial p}{\partial y} + \frac{\mu_{nf}}{\rho_{nf}}\nabla^2 v \tag{3}$$

$$\mathrm{S}.\nabla \mathrm{T} = \frac{\alpha_{nf}}{\rho_{nf} C_{p_{nf}}}\nabla^2 \mathrm{T} \tag{4}$$

$$\text{with} \quad \mathrm{s} = (u,\ v),\ \nabla = \mathrm{i}\frac{\partial}{\partial \mathrm{x}} + \mathrm{j}\frac{\partial}{\partial \mathrm{y}}$$

Here, Re (Akbari (a) et al. 2016), Nu (Sheikholeslami et al. 2016), Δp, P_p and C_f (Leng et al. 2015), R have been formulized as follows:

$$\mathrm{Re} = \frac{\rho u_{in} d}{\mu} \tag{5}$$

$$Nu = \frac{hd}{k_f} \tag{6}$$

$$C_f = \frac{\tau_l}{2\rho u_{in}^2} \tag{7}$$

$$\nabla p = p_{out} - p_{in} \tag{8}$$

$$R = \frac{1}{h_d + h_u} \frac{\left(T_{\max} - T_{\min}\right)}{25000} \tag{9}$$

Here $\rho, \mu, h, \alpha,\ nf, f, p_{out},$ and p_{in} designate density, dynamic viscosity, convective HT coefficient, thermal diffusivity, nanofluid, base fluid, pressure at outlet, pressure at inlet respectively.

3.1 Nanofluid characteristics

The following formulations are utilized to calculate the nanofluid density (ρ_{nf}), and specific heat capacity ($(\rho C_p)_{nf}$) as per the studies of Nikkah et al. (2015).

$$\rho_{nf} = (1-w)\rho_f + w\rho_{n_p} \tag{10}$$

$$\left(\rho C_p\right)_{nf} = (1-w)\left(\rho C_p\right)_f + w\left(\rho C_p\right)_{n_p} \tag{11}$$

To calculate the effective dynamic viscosity of nanofluids, Brinkman correlation has been utilized (Brinkman 1952):

$$\mu_{ef} = \frac{\mu_f}{(1-w)^{2.5}} \tag{12}$$

Using the formula of Aminossadati et al. (2011), effective thermal diffusion coefficient (α_{nf}) of nanofluid has been calculated:

$$\alpha_{nf} = \frac{k_{eff}}{\left(\rho C_p\right)_{nf}} \tag{13}$$

The following expression has been used to evaluate the effective thermal conductivity of nanofluid for suspensions with spherical particles (Patel et al. 2005):

$$k_{eff} = k_f \left[1 + \frac{k_{n_p} A_{n_p}}{k_f A_f} + c k_{n_p} Pe \frac{A_{n_p}}{k_f A_f}\right] \tag{14}$$

Here, the expressions of $c = 36{,}000, \frac{A_{np}}{A_f}$ and Pe have been calculated as per the studies of Patel et al. (2005).

$$\frac{A_{n_p}}{A_f} = \frac{d_f}{d_{n_p}} \frac{w}{1-w} \tag{15}$$

$$Pe = \frac{u_{n_p} d_{n_p}}{a_f} \tag{16}$$

Where, d_f (water molecule diameter) = 2Å, carbon nanoparticle molecule diameter $d_{n_p} = 50$ nm and Brownian motion velocity of nanoparticles (u_{n_p}) which calculated by the following expression:

$$u_{n_p} = \frac{2k_b T}{\pi \mu_f d_{n_p}^2} \tag{17}$$

Where κ_b is taken as per the studies of Kuppusamy et al. (2014).

Type	w%	$\rho(\frac{kg}{m^3})$	μ $(Pa.s)$	C_p	k
water	0.00	995.8	0.000765	4178	0.62
water +CN	0.12	1003	0.00078	4178	0.68
Water+CN	0.25	1008	0.000795	4178	0.75

Table 1. Nanofluid properties.

grid	zone 1	zone 2	elements	average C_p
1	30 × 10	750 × 30	22,910	1.8852
2	60 × 20	1500 × 60	91,220	1.88930
3	120 × 40	3000 × 120	3,64,840	1.889301

Table 2. Grid study for pure water (w% = 0.00).

3.2 Computational procedures, Grid independency test, and Validation of code

Ansys Fluent has been used for simulation and visualization purposes. Despite some compelling features of the finite volume method (FVM), the lower order interpolation of the convective terms in the governing equations causes several unwanted numerical effects. To avoid those, the QUICK scheme (Leonard's 1979) has been used for spatial discretization of convective terms in the momentum equation. It is an upwind scheme that is accurate up to 3rd order for the advection terms but only to 2nd order for all other terms. SIMPLEC algorithm (van Doormaal et al. 1984, Ternik et al. 2006) resolves velocity and pressure coupling. As a result, using the SIMPLEC technique (van Doormaal et al. 1984, Ternik et al. 2006), updated velocity and pressure fields satisfying exactly mass balance (the continuity equation) and essentially discrete momentum equations have been found. To study the effect of the mesh size, a grid test has been performed at $Re_n = 60$ as illustrated in Fig. 2(a-b). Fig. 2(a-b) represents the variation of pressure coefficients with the number of elements. Fig. 2(b) stated that 91, 220 number of cells are enough for future analysis. Moreover, Fig. 2(a) depicts a good agreement between three different meshes (Table 2). Furthermore, from Fig. 2(a), it can be seen that grid 2 can be taken for further analysis. Validation has been done with the studies of Oliveira (2003) and Ternik et al. (2006) by analysis of primary vortex length (Fig. 3a) and normalized vortex length (Fig. 3b), which shows a good agreement (Figs. 3(a-b)) of these with those of the present models. The configured geometry has been segregated into two different parts with the aid of fine mesh (Fig.4).

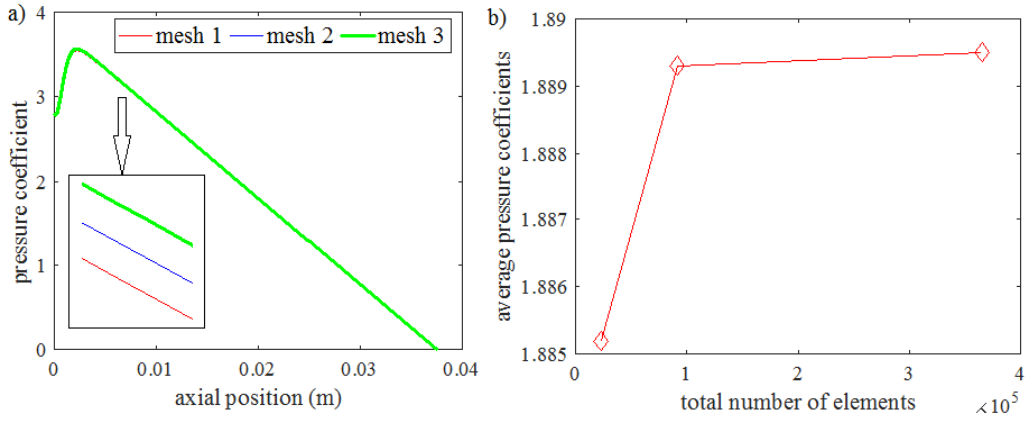

Fig. 2. Graphs of (a) pressure coefficients vs axial position and (b) average pressure coefficients vs total number of elements.

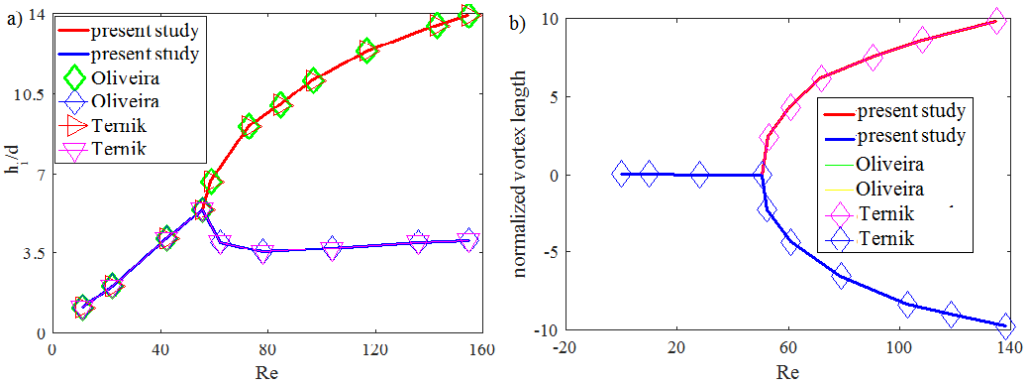

Fig. 3. Graphs of (a) length of primary vortex and (b) length of normalized vortex vs. Re.

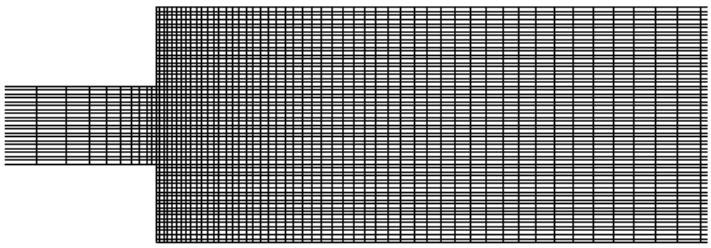

Fig. 4. Mesh geometry.

4. Results and Discussions

4.1 Flow phenomena for w% = 0.00

Figures 5, 6 (a-c) present the axial velocity and static temperature profiles for $Re = 1$, 50 and 130, respectively. Near the expanded section, it is found that the rate ofnon-viscous core

penetration increases with the increase of inflow velocity (Fig. 5). Moreover, it is observed that as the increase of *Re*, flow transition changes symmetric to asymmetric due to pressure drop and the flow moves to the outlet section of the channel. Furthermore, Fig. 5 shows that low pressure zones are formed due to the increase of flow velocity and pressure drop. In Fig.6, it is demonstrated that the static temperature reduces as thein flow velocity increases. Due to the enhancement of cooling fluid momentum and the increase of Re, the variation of temperature and kinetic energy is reduced near the expanded section of the channel. Near the upper wall, it is found that an increase of Re causes the reduction of thermal boundary layer thickness (Fig. 6). Furthermore, it is also apparent that HT rate rises as Re increases.

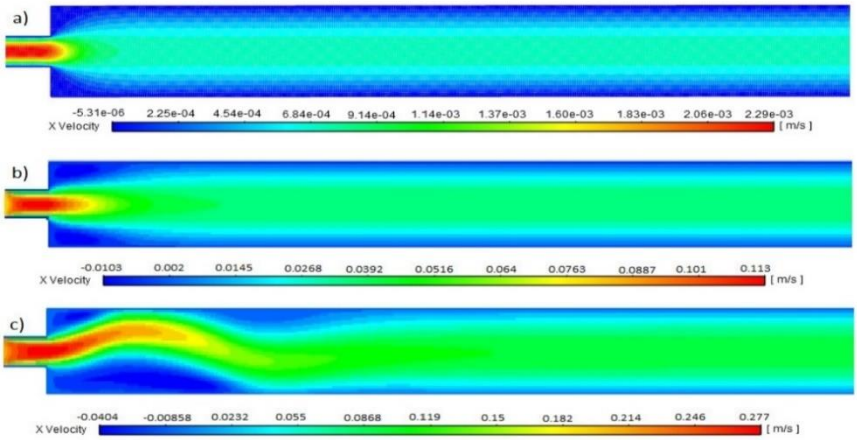

Fig. 5. Axial velocity contour (a) $Re = 1,50$ and (c) 130.

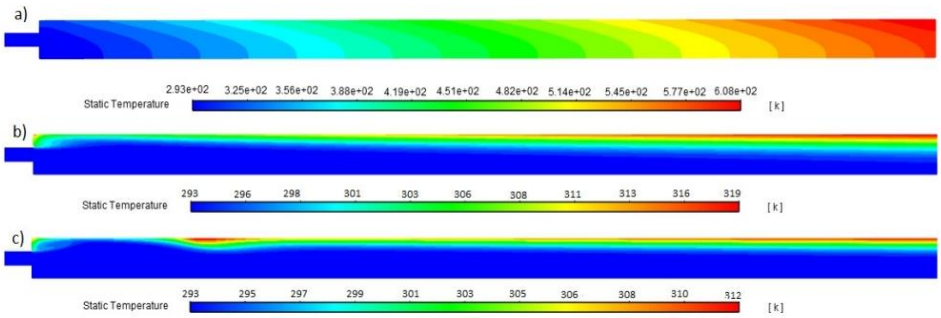

Fig. 6. Static temperature profile at (a) $Re = 1,50$ and (c) 130.

4.2 Effect of w%

Figures 7 and 8 show the velocity streamlines for three various w%, such as 0, 0.12, and 0.25, respectively. At $Re = 50$ (fig. 7), and $Re = 130$ (Fig. 8) it is shown that the enhanceof Re causes an enhancement in the length of vortex. From the color plot of Figs.7, 8(a-c), it is clearly observed that the flow velocity increases as the weight percentage of nanoparticles increases. Figure 9 presents the bifurcation diagram for different weight percentage with respect to different values of *Re*. Moreover, for all the three taken weight percentages, it is found that the bifurcation of flow symmetry starts to break when $Re \leq 50$, which is shown in Figs.7(a-c) and

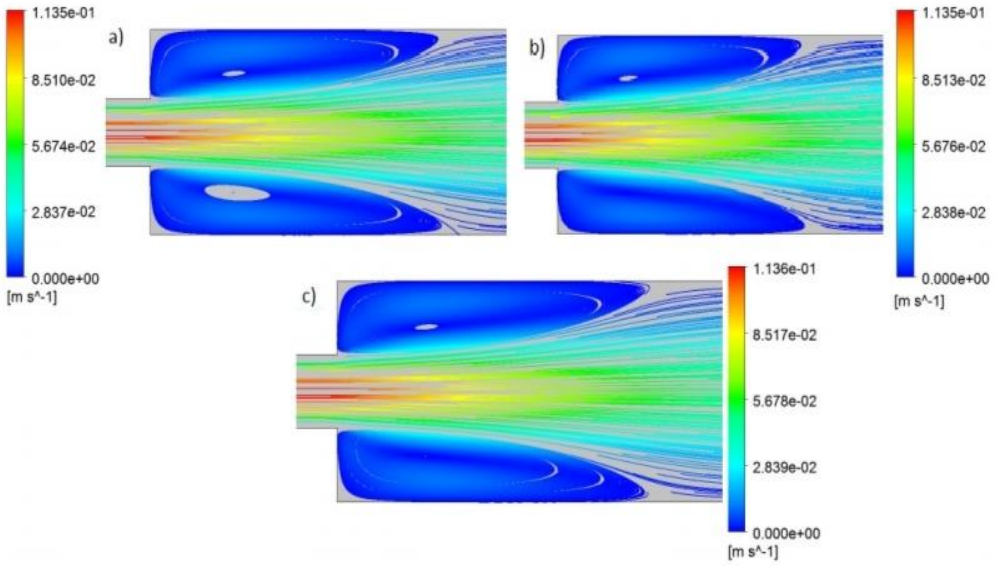

Fig. 7. Velocity streamlines for (a) $w\% = 0$, (b) 0.12, and (c) 0.25 at $Re = 50$.

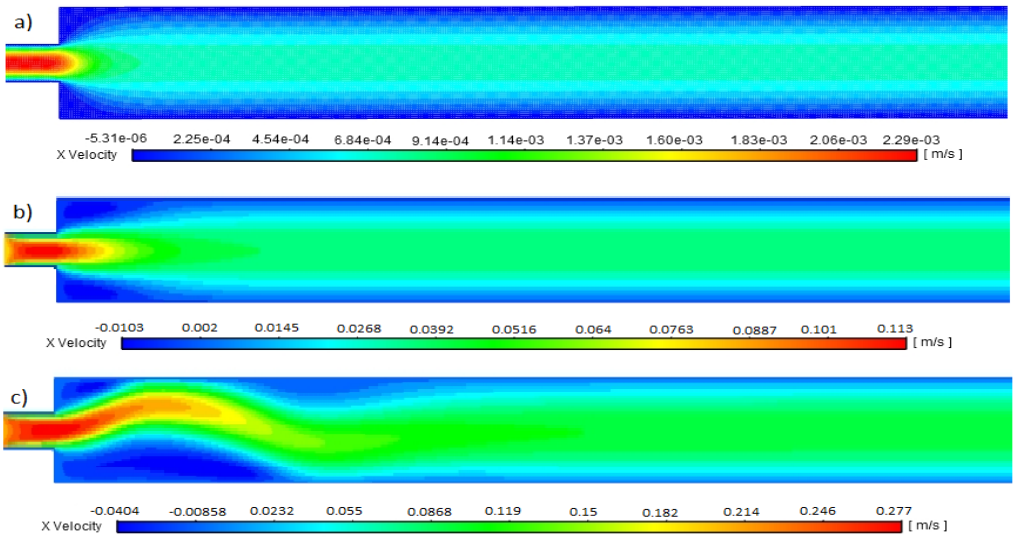

Fig. 8. Velocity streamlines for (a) w% = 0, (b) 0.12, and (c) 0.25 at $Re = 130$.

It is found that different lengths of corner vortices exist when $Re > 50$. Further investigations revealed that $Re_{cr} = 49.8$ for $w\% = 0$, but for $w\% = 0.12$, Re_{cr} becomes 49.93 and also $Re_{cr} = 50$ for $w\% = 0.25$, which are clearly shown in Fig. 9. Re_{cr} is the point of exchange of stability. Therefore, it is observed that the value of Re_{cr} rises with an increment in w%. For different values of Re, pressure drop characteristics have been presented in Fig. 10(a). It is found that pressure drop gradually increases with the increase of Re. Moreover, for w% = 0.00, 0.12, 0.25, it is observed that the pressure drop remains approximately the same at Re = 1. It has also been investigated that pressure drop becomes more pronounced at w% = 0.25 rather than w% =

0.00. Therefore, these phenomena induce the decrease of momentum and an increase in pressure drop by enhancing the velocity of fluid in indirect paths. For three different w% values, the profile of thermal resistance factor has been shown in Fig. 10(b), at three different values of Re. Rcan be described as the efficient parameter to calculate the amount of thermal resistance. It is observed that the improvement of HT causes the significant decrease of R with the increase of Re. Moreover, it is also found that the amount of R becomes more pronounced at $Re = 1$, as compared to $Re = 130$.

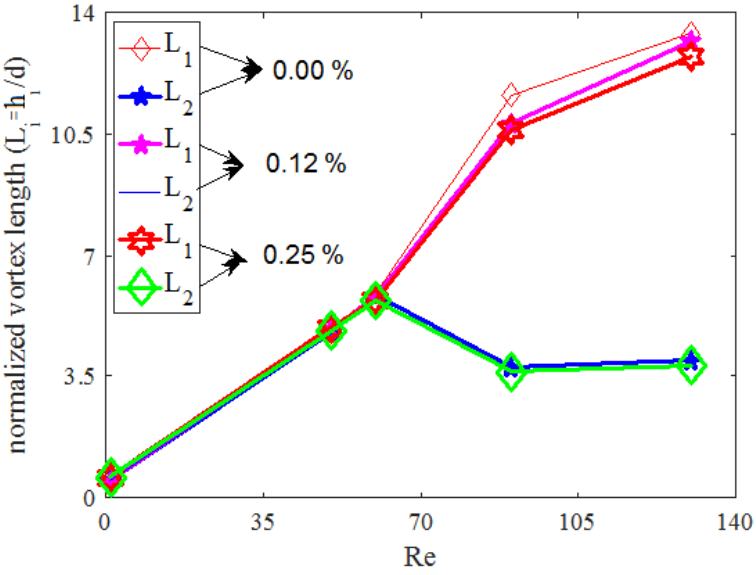

Fig. 9. Bifurcation diagram for different weight percentages at different Re.

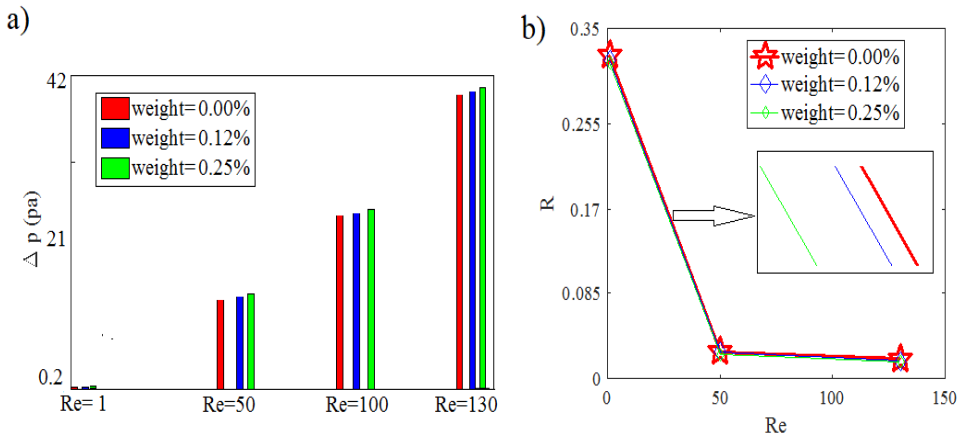

Fig. 10. Plots of (a) pressure drop, (b) R for various Re.

4.3 Thermal behavior

For different Re, Fig. 11 (a-b) depicts the variation of C_f and Nu(x) along the upper wall for $w\% = 0.00$. Due to the presence of cross-sectional area and the variation of velocity on the channel, friction coefficient becomes more pronounced at higher values of Re (Fig. 11(b)). Moreover, it is also investigated that shear stress becomes higher as the axial velocity increases which causes the enhancement of friction coefficient. Along the hot channel wall, the variation of local Nusselt number has been presented in Fig.11(a) for three weight percentages at different values of Re. At higher values of *Re*, it is studied that the profile of Nusselt number becomes more pronounced due to the increase of convective HT coefficient. As a result, rapid energy exchange of the cooling fluid causes an increase of HT rate. Moreover, it has also been studied that HT rate and Nu decreases at the beginning of the expanded section due to the increase rate of HT between fluid weight percentage and upper wall and decrease rate of thermal boundary layer. For various *Re*, the variation of friction factor has been shown in Fig. 12(a) for different values of $w\%$. As it is seen that, for all taken w%, friction factor reduces as the increase of Re. Due to the decrease of boundary layer thickness and frictional effects the rate of flow reduces. Moreover, it is also observed that nanofluid particles interact with the wall surface for low values of Re.However, as the increase of Re, chances the interaction with the wall surface becomes higher. Furthermore, it is also observed that for sufficiently small values of w, there is an increase in the values of higher momentum at the upper wall. Figure 12(b) presents the profile of Nu_{avg} for different weight percentages at $Re = 1$, and $Re = 130$.

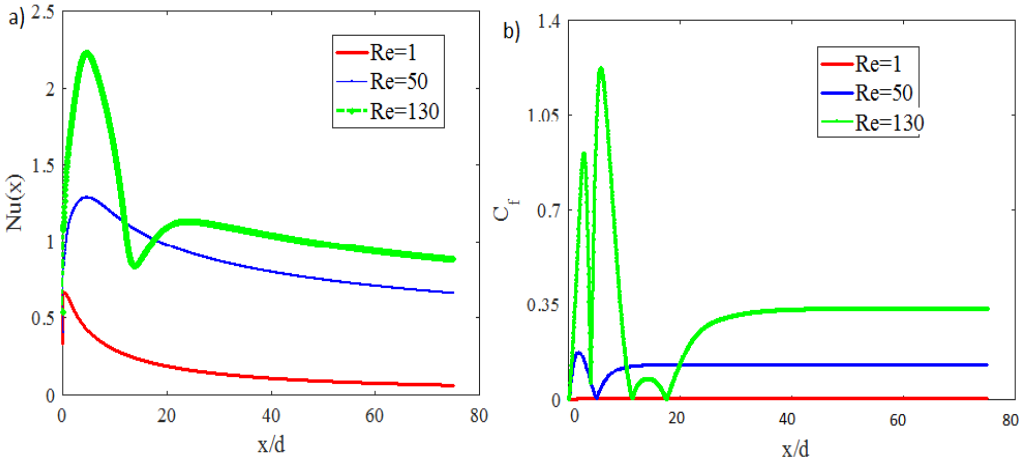

Fig. 11. Plots of (a) Nu(x) and (b) C_f at various Re.

Further study asserts that increase in the values of h and w% cause the increase of Nu_{avg}. Figure 12(b) shows the linear relationship between Nu_{avg} and Re. For different values of Re, pumping power has been shown in Fig. 12(c) for three values of w%. Strong pumps are required to achieve an adequate fluid velocity. Moreover, for all values of Re, it is investigated that pumping power increases with the increase of w% due to the presence of nanoparticles in the cooling fluid. Furthermore, it is observed that a high rate of pumping power is required for w% = 0.25 (high density and high viscosity of fluid) as compared to w% = 0.00.

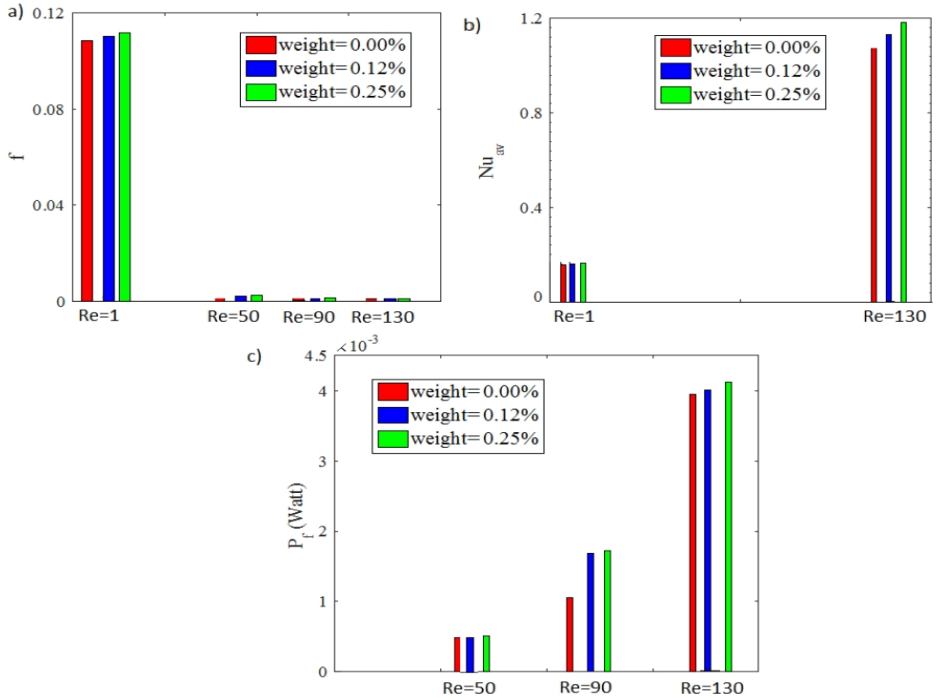

Fig. 12. Plots of (a) f, (b) Nu_{avg}, and (c) Pp at various Re.

Conclusions

It is observed that with the increase of Re flow transition changes from symmetric to asymmetric. Moreover, for three different values of weight percentages, it has been revealed that two different lengths of corner vortices exist when $Re \leq 50$. But for $Re > 50$, flow bifurcation breaks the symmetry.

It has been also investigated that $Re_{cr} = 49.8$ for w% = 0.00, but for w% = 0.12, Re_{cr} becomes 49.93 and also $Re_{cr} = 50$ for w% = 0.25. Therefore, it is concluded that an increase of weight percentage causes the increase of Re_{cr}. It is also found that the increase of velocity causes the increase of friction coefficient, pressure drop as well as average Nusselt number. Moreover, it has also been noted that pressure drop becomes more enhanced at w% = 0.25as compared to w% = 0.00.

It is found that friction factor decreases with increase of Re. In addition, itis concluded that an increase of Re causes the increase of Nu_{avg}. Pumping power elevated with the rise of weight percentages and Re. Furthermore, it is also revealed that more pumping power is needed for w% = 0.25 as compared to w% = 0.00. Further investigation revealed that thermal resistance factor decreases with the increase of Re.

Conflict of interest

None.

Acknowledgements

The authors are very grateful to the reviewers for their valuable comments.

References

Abu E (2008). Application of nanofluids for heat transfer enhancement of separated flows encountered in a backward facing step, Int. J. Heat Fluid Flow, 29 (1), 242-249.

Akbari (a) OA, Karimipour A, Toghraie D, Karimipour A (2016). Impact of ribs on flow parameters and laminar heat transfer of Water- aluminum oxide nanofluid with different nanoparticle volume fractions in a three-dimensional rectangular microchannel, AdvMechEng, 7, 1-11.

Akbari (b) OA, Toghraie D, Karimipour A (2016). Numerical simulation of heat transfer and turbulent flow of water nanofluids copper oxide in rectangular microchannel with semi attached rib, Adv. Mech. Eng, 8(4), 1-25.

Alavi A, Safaei RM, Mahian O, Goodarzi M, Dahari M, Yarmand Y, Wongwises H (2015). A hybrid finite element/finite difference scheme for solving the 3-d energy equation in transient non-isothermal fluid flow over a staggered tube bank, Numer. Heat Tran, 68, 169-183.

Akbari (c) OA, Karimipour A, Toghraie D, Safaei R. M, Alipour G, Dahari M (2016). Investigation of Ribs height effect on heat transfer and flow parameters of laminar water-Al_2O_3 nanofluid in a two-dimensional rib-microchannel, Appl Math Comp, 290, 135-153.

Afrouzi HH, Farhadi M, Mehrizi AA (2013). Numerical simulation of microparticles transport in a concentric annulus by Lattice Boltzmann Method, Adv. Powder Technol, 24 (3), 575-584.

Andreozzi A, Manca O, Nardini S, Ricci D (2016). Forced convection enhancement in channels with transversal ribs and Nanofluids, ApplThermEng, 98, 1044-1053.

Aminossadati MS, Raisi A, Ghasemi B (2011). Effects of magnetic field on nanofluid forced convect ion in a partially heated microchannel, Int. J. Nonlinear Mech, 46, 1373–1382.

Behnampour A, Akbari OA, Safaei RM, Ghavami M, Marzban A, Sheikh Gh R, Zarringhalam, M, Mashayekhi R (2017). Analysis of heat transfer and nanofluid fluid flow in microchannels with trapezoidal, rectangular and triangular shaped ribs, Physica, 91, 15-31.

Bardenhagen KA, Esfe M, Safaei M (2014). Mixed convection of copper-water nanofluid in a shallow inclined lid driven cavity using the lattice Boltzmann method, Physica A, 402, 150-168.

Brinkman CH (1952). The viscosity of concentrated suspensions and solution, J. Chem. Phys, 20, 571–581.

Gravndyan Q, Akbari OA, Toghraie D, Marzban A, Mashayekhi R, Pourfattah F (2017). The effect of aspect ratios of rib on the heat transfer and laminar water/TiO_2nanofluid flow in a two dimensional rectangular microchannel, J MolLiq, 236, 254-265.

Gholami RM, Akbari OA, Marzban A, Toghraie D, Shabani GAS, Zarringhalam M (2018). The effect of rib shape on the behavior of laminar flow of oil/MWCNT nanofluid in a rectangular microchannel, Journal of Thermal Analysis and Calorimetry, 134, 1611-1628.

Heidary H, Kermani MJ (2010). Effect of nano-particles on forced convection in sinusoidal wall channel, IntCommun Heat Mass, 37, 1520-1527.

Kuppusamy RN, Mohammed HA, Lim WC (2014). Thermal and hydraulic characteristics of nanofluid in a triangular grooved microchannel heat sink (TGM-CHS), Appl. Math. Comput, 246, 168–183.

Jung JY, Oh HS, Kwak HY (2009). Forced convective heat transfer of nanofluids in microchannels, Int J Heat Mass Tran, 52, 466-472.

Karimipour A, Nezhad AH, Dorazio A, Ebrahim S (2013). The effects of inclination angle and Prandtl number on the mixed convection in the inclined lid driven cavity using lattice Boltzmann method, J TheorApplMech, 51, 447-462.

Karimipour (b) A, Alipour H, Akbari OA, Semiromi DT, Esfe MH (2015). Studying the effect of indentation on flow parameters and slow heat transfer of water-silver nano-fluid with varying volume fraction in a rectangular two-dimensional microchannel, Indian J SciTechnol, 8(15), 1-13.

Leng C, Wang DX, Wang HT (2015). An improved design of double-layered microchannel heat sink with truncated top channels, Appl. Therm. Eng, 79: 54-62.

Leonard PB (1979) A Stable and accurate convective modelling procedure based on quadratic upstream interpolation, Comp. Methods Appl. Mech. Eng, 19, 59-98.

Li YF, Xia GD, Ma DD, Jia YT, Wang J (2016). Characteristics of laminar flow and heat transfer in microchannel heat sink with triangular cavities and rectangular ribs, Int J Heat Mass Transf, 98, 17-28.

Moshizi SA, Malvandi A, Ganji DD (2014). A two-phase theoretical study of Al_2O_3-water nanofluid flow inside a concentric pipe with heat generation/absorption, Int J ThermSci, 84, 347-357.

Moghiman M, Rahmanian B, Safaei RM, Goodarzi M (2008). Numerical investigation of heat transfer in circular perforated plates exposed to parallel flow and suction, Int J Adv Des ManufTechnol, 1(3), 43-56.

Mahmoudi HA, Pop I, Shahi M (2012). Effect of magnetic field on natural convection in triangular enclosure filled with nanofluid, Int. J. Therm. Sci, 59, 126-140.

Nikkhah N, Karimipour A, Safaei MR, Forghani-Tehrani P, Goodarzi M, Dahari M, Wongwises S (2015). Forced convective heat transfer of water/functionalized multi-walled carbon nanotube nanofluids in a microchannel with oscillating heat flux and slip boundary condition, Int. Commun. Heat Mass Tran, 68, 69-77.

Oliveira JP (2003). Asymmetric flows of viscoelastic fluids in symmetric planar expansion geometries, J. Non-Newtonian Fluid Mech, 114, 33-63.

Patel EH, Sundararajan T, Pradeep T, Dasgupta A, Dasgupta N, Das KS (2005). A micro-convection model for thermal conductivity of nanofluids, Pramana-J. Phys, 65, 863–869.

Parsaiemehr M, Pourfattah F, Akbari OA, Toghraie D, Sheikhzadeh GH (2018) Turbulent flow and heat transfer of water/ Al_2O_3nanofluid inside a rectangular ribbed channel, Phys E, 96, 73-84.

Peyghambarzadeh SM, Hashemabadib SH, Chabia RA (2014). Performance of water based CuO and Al_2O_3nanofluids in a Cube alloy heat sink with rectangular microchannels, Energ Convers Manage, 86, 28-38.

RamReddy C, Murthy VP, Chamkha JA, Rashad AM (2013). Soret effect on mixed convection flow in a nanofluid under convective boundary condition, Int. J. Heat Mass Tran, 64, 384-392.

Raisi A, Ghasemi B, Aminossadati MS (2011). A numerical study on the forced convection of laminar nanofluid in a microchannel with both slip and no-slip conditions, Numer Heat Tr A: Appl, 59, 114-129.

Sarlak R, Yousefzadeh S, Akbari OA, Toghraie D, Sarlak S, Assadi F (2017). The investigation of simultaneous heat transfer of water/2O3 nanofluid in a close enclosure by applying homogeneous magnetic field, Int. J. Mech. Sci, 133, 674-688.

Saha S, Raut S, Das NA (2021). Analysis of thermal enhancement in a trapezoidal baffled channel with various formations of an outlet, J. Serbian Society for Computational Mechanics, 15(1), 24-36.

Sheikholeslami M, Gorji-Bandpy M, Ganji DD (2016). Effect of discontinuous helical turbulators on heat transfer characteristics of double pipe water to air heat exchanger, Energy Convers Manag, 118, 75-87.

Ternik P (2009). Planar sudden symmetric expansion flows and bifurcation phenomena of purely viscous shear-thinning fluids, J. Non-Newtonian Fluid Mech, 157, 15- 25.

Toghraie D, Shirani E (2019). Numerical simulation of water/ alumina nanofluid mixed convection in square lid-driven cavity, Effect of magnetic field using a two-phase model, International Journal of Numerical Methods for Heat & Fluid Flow, 30(5), 2782-2807.

Van Doormal KH, Malalasekera W (1985). Enhancement of The SIMPLE Method for predicting incompressible fluid flows, Numerical Heat Transf, 7, 147-163.